Journal of Climate Change
ISSN 2395-7611 Volume 12 (2026) No. 1. pp. 88–106

https://doi.org/10.70917/jcc-2026-006
Article

A Multimodel Ensemble Approach for Spatiotemporal Variability and Trend Analysis of Extreme Precipitation Indices Using CMIP6 Climate Model Projections in Mono River Basin

Joselyne Lisbeth Godonou[1,2], Jérôme Enagnon Ahouandjinou [2,3,4,*] and Edia Flavien Dovonou [2]

1 Ecole Doctorale des Sciences Agronomiques et de l'Eau (EDSAE), University of Abomey-Calavi, Abomey-Calavi BP : 526 UAC, Benin
2 National Water Institute (NWI), University of Abomey-Calavi, Abomey-Calavi BP: 526 UAC, Benin
3 International Chair in Mathematical Physics and Applications (ICMPA-UNESCO Chair), University of Abomey-Calavi, Abomey-Calavi BP: 526 UAC, Benin
4 Centre for Applied Water Research (CAWR), Abomey-Calavi BP 2147, Benin
* Correspondence author: jeromeahouandj@gmail.com

Abstract: Rainfall extremes in the Mono River Basin (MRB) exhibit marked spatial and temporal heterogeneity, and their accurate characterization is essential for sustainable water governance and natural hazard mitigation. This study evaluated the capacity of a multimodel ensemble built from CMIP6 General Circulation Models (GCMs) to capture and project the spatiotemporal evolution of extreme precipitation indices across the MRB. The methodological framework integrates three successive components: a performance-based selection of GCMs using a multicriteria ranking score, a systematic bias adjustment using the Quantile Delta Mapping (QDM) technique, and the construction of a weighted multi-model ensemble (MME) using inverse RMSE weighting. The ranking procedure, applied to 10 CMIP6 GCMs against CHIRPS satellite-derived as reference data, led to the selection of five top-performing models. Trend analyses of four extreme precipitation indices (Rx1day, SDII, PRCPTOT, and R20) were subsequently conducted over the projection period of 2030-2060 under SSP2-4.5 and SSP5-8.5 scenarios, using both the Modified Mann-Kendall (MMK) test and Innovative Trend Analysis (ITA). The results indicate that the ensemble configuration systematically outperformed the individual GCMs in reproducing the observed hydroclimatic variability, as evidenced by the superior RMSE, R^2, NSE, and KGE scores. For the spatial aspect, the results reveal clear spatial variability in extreme precipitation over the MRB, with stronger positive trends mainly in the central and southern regions. Extreme precipitation indices indicate the intensification of extreme rainfall, particularly in downstream areas. The magnitude of these changes amplified considerably under SSP5-8.5, indicating the sensitivity of MRB hydrology to emission pathway assumptions. The obtained results enable us to provide valuable insights for improving the understanding of the extreme precipitation indices distribution for informing flood risk assessment, agricultural planning, and integrated water resource management in the basin under future climate conditions.

Keywords: CMIP6, extreme precipitation indices, Climate change, Spatiotemporal variability, Trend analysis

1. Introduction

Climate change and its variability have intensified globally over recent decades and pose substantial risks to natural and human systems (Martinich et al., 2019; Upadhyay et al., 2020), and its frequency has decreased compared to the past (Asare-Nuamah, 2021). This can be clearly seen in the increasing temperatures, more frequent droughts, and flood events, and spatiotemporal changes of rainfall in many regions of the world (Taye et al., 2021). West Africa is a region that faces considerable hydroclimatic extremes and is expected to be among the areas most affected by climate change (De Longueville et al., 2020; Sylla et al., 2015). According to (Gandomé et al. 2021) and (Klutse et al. 2021), there has been an intensification in extreme weather events and alterations in rainfall patterns due to climate change in West Africa. The damage caused by these events to natural systems and human communities tends to be far greater than that caused by ordinary weather fluctuations.

The Mono River Basin (MRB), a transboundary catchment between Benin and Togo, is of major socioeconomic importance and is greatly influenced by climate variability because of its pronounced rainfall seasonality and exposure to hydrological extremes (Akinsanola et al., 2015; Amoussou et al., 2020; Ogbu et al., 2020). Most residents rely on farming as their main source of income, and because this activity is closely linked to rainfall patterns, it consequently affects the local economy. As a result, any shifts in rainfall patterns may impact crop yield production, potentially causing food insecurity. Additionally, in the MRB, flooding tends to coincide with the wet season, thereby amplifying its effects on local communities (Lawin et al., 2019). Reliable understanding of these climate extremes variability at local scale is very important for effective mitigation strategies.

In the past, a variety of research has been undertaken to analyze these climate extremes variability across the MRB. For example, (Akinsanola et al. 2015) assessed three CORDEX-Africa regional climate models (RegCM4, RCA4, CCLM4) for estimating summer monsoon in West Africa. Although these models broadly captured spatial and seasonal precipitation patterns, they exhibited systematic biases of underestimation over the Gulf of Guinea and overestimation over the Sahel with variable skill across sub-regions. These findings highlight the persistent uncertainties in regional climate modelling across West Africa, underscoring the need for bias correction approaches in hydrological impact studies. (Lawin et al. 2019) investigated future climate variability in the MRB using the REMO2009 model and reported that annual precipitation and temperature are projected to exhibit high variability with a significant increasing trend. (Koubodana et al. 2019) emphasized that, temperature is projected to rise significantly across the basin, while rainfall will decrease slightly under the RCP4.5 and RCP8.5 scenarios in the MRB. Houngue et al. (2022) utilized CORDEX regional climate models and employed a TOPSIS multi-criteria method to identify the most effective models for the Mono River Basin. Their findings suggest that by 2070, annual temperatures will increase by approximately 1-1.5 °C under the RCP4.5 and RCP8.5 scenarios, while annual precipitation is predicted to experience a slight, though statistically insignificant, decline. Moreover, (Gandomé et al. 2021) and (Klutse et al. 2021) contributed significantly to the general understanding of climate patterns using CMIP6 models over West Africa; however, they rarely capture watershed-scale variability and local microclimatic patterns both of which directly shape agricultural and water resource dynamics. Therefore, rainfall is expected to become more intense with shorter rainy seasons, potentially increasing flood risk in the basin. Overall, these studies have employed statistical analyses of rainfall and climate indices from the Expert Team on Climate Change Detection Indices (ETCCDI) (Dosio et al., 2020). These methodologies have collectively advanced our understanding of the evolution of hydroclimatic processes across the basin and the factors influencing these transformations. While CMIP5-based studies have broadly examined climate variability across the MRB, persistent challenges remain, such as limitations in the availability and quality of historical reference data to capture fine-scale spatial variability. In addition, CMIP5 models use representative concentration pathway scenarios that do not consider socioeconomic development in the region. Beyond data and methodological limitations, the variability in time and space of extreme precipitation indices and the climate model framework selection which takes into account the seasonal variability, trend, and accuracy of the models across the MRB, have received little systematic attention in the existing literature. Therefore, assessing future changes in rainfall patterns using more accurate data, methods, and models is important for understanding the dynamics of extreme precipitation indices and managing their impacts on water resources.

This study addresses knowledge gaps by investigating the spatiotemporal variability and trend of extreme precipitation indices framework using multi-model ensemble (MME) with CMIP6 GCMs over the MRB. Additionally, many previous works have considered rainfall gauge data, which are both temporally short and spatially sparse, as reference data, the present study addresses three interconnected objectives: (i) to assess the performance of 10 CMIP6 GCMs in reproducing historical precipitation and temperature characteristics over the MRB during the baseline period 1985–2014, using the Climate Hazards Group InfraRed Precipitation with Station data (CHIRPS) as observational reference; (ii) to construct and validate a weighted Multi-Model Ensemble (MME) from the best-performing models following QDM bias correction; and (iii) to analyze the spatiotemporal variability and trends of four extreme precipitation indices Rx1day, SDII, PRCPTOT, and R20 over the projection period 2030–2060 under SSP2-4.5 and SSP5-8.5 scenario. By integrating statistical trend methods (MMK and ITA) with spatial analysis, this work aims to deliver actionable climate intelligence for water resource planning in the MRB under future emission scenarios. Three distinctive contributions should be highlighted: (i) the integration of a five-indicator multi-criteria model selection, Quantile Delta Mapping (QDM) bias correction, and an inverse-RMSE weighted multi-model ensemble, a methodological combination not yet applied in the MRB; (ii) a dedicated focus on ETCCDI extreme precipitation indices, which are more informative than climatological means for hydrological risk management; (iii) the cross-validation of trends using both MMK and ITA, enabling the detection of the statistical significance of monotonic trends together with their internal structure across sub-intervals.

2. Materials and methods

2.1. Study area

The Mono River Basin spans an area of 27,822 km², divided between the West African nations of Togo and Benin. Geographically, it is situated between latitudes 06°16’N and 09°20’N, and longitudes 0°42’E and 2°25’E (Figure 1.). The majority of the basin, covering 21,750 km², is located within Togo, while Benin encompasses 6,072 km². The basin sits under a subequatorial climate in the south below 7°N with two rainy and two dry seasons; above that threshold, the regime shifts to tropical, with a single rainy season covering the central and northern sections (Lawin et al., 2019; Amoussou, 2010). Between 7°N and 8°N, the rainfall regime shifts to a transitional mode, a single peak builds in July and holds through September. Subequatorial parts of the basin record two distinct peaks in June and October, while tropical zones see a single maximum in August. Mean annual rainfall ranges from around 1,100 mm in the south to roughly 1,300 mm northward (Lawin et al., 2019).

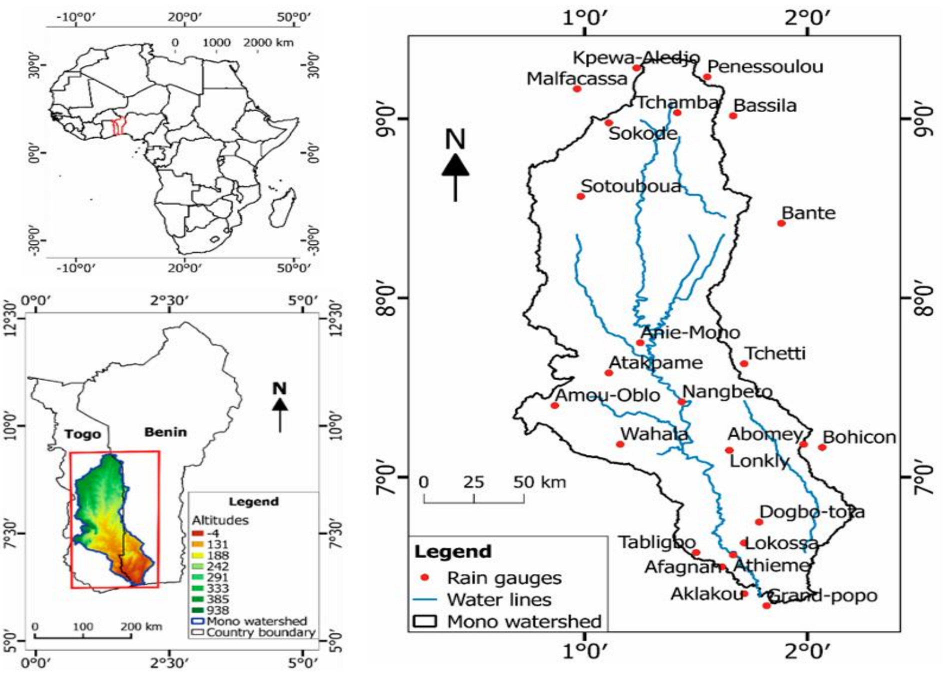

Figure 1. Study area

2.2. Data used

Daily precipitation and near-surface temperature outputs from 10 CMIP6 GCMs were used in this study (Table 1). Model simulations were obtained for two shared socioeconomic pathways: SSP2-4.5, representing an intermediate emissions trajectory consistent with moderate sustainability efforts, and SSP5-8.5, reflecting a high-emissions development pathway. These two contrasting scenarios were selected to bracket the plausible range of future hydroclimatic responses in the MRB, enabling a sensitivity assessment of extreme precipitation indices to radiative forcing intensity. The historical simulation period spans 1985–2014, while future projections cover 2030–2060. To evaluate how well the various CMIP6 models simulate daily precipitation characteristics, the CHIRPS daily precipitation dataset was employed as a reference for the years 1985–2014, with a resolution of 0.5 °× 0.5 °. For temperature data, we utilized the spatial daily mean temperature provided by the Togo Agency of Meteorology for the baseline period of 1985-2014. As CHIRPS is delivered pre-controlled by the Climate Hazards Center, we only verified the statistical consistency of the series (absence of negative values, daily distribution consistent with regional climatology). For the temperature data, these data come from the synoptic stations of the Togolese and Beninese national meteorological services and are of good quality. We verified inter-annual consistency and distribution of daily intensities.

Table 1. Specification of climate models used in this work

CMIP6 model	Resolution	Institution	Country
ACCESS-CM2	1.25° x 1.875°	CSIRO-ACCESS	Australia
BCC-CSM2-MR	1.125° × 1.125°	BCC, CMA	China
CNRM-CM6-1	1.406° × 1.406°	CNRM	France
CNRM-ESM2-1	1.4° x 1.4°	CNRM_CERFACS	France
GFDL-ESM4	1° × 1.125°	GFDL	USA
MIROC6	1.406° × 1.406°	MIROC	Japan
MPI-ESM1-2-HR	0.938° × 0.938°	MPI-M	German
MPI-ESM1-2-LR	1.875° × 1.875°	MPI-M	German
NorESM2-MM	0.9424° × 1.25°	NCC	Norway
TaiESM1	0.938° × 1.25°	RCEC	China

2.3. Methods

2.3.1. Selection of the best-performed CMIP6 models

All 10 CMIP6 GCMs used in this study operate at different spatial resolutions. To allow a consistent comparison between datasets with different spatial resolutions, a bilinear interpolation method was applied to regird all CMIP6 GCMs models' output data to match the spatial resolution of CHIRPS data. For temperature data, no spatial interpolation was applied. This is because we focus exclusively our analysis on temporal basin-averaged of temperature time series. The observed temperature dataset was constructed as the spatial average of three synoptics meteorological stations in Mono River basin with Thiessen method. Climate models often share structural similarities, which means they cannot be treated as truly independent. To account for this, a weighting approach is applied so that the ensemble output reflects what a set of genuinely independent models would produce on average. By assigning greater weight to well-performing models and discarding those that reproduce climate patterns poorly, weighted MMEs yield estimates that are more precise and trustworthy (Shuaifeng & Xiaodong, 2022). This study aimed to select at least five top-performing GCMs to build a multimodel ensemble suited to the analysis of extreme precipitation indices. No consensus has yet been reached regarding the optimal number of GCMs required to form a robust MME. Five GCMs were retained for this purpose. The choice of five GCMs is not arbitrary but is supported by three converging findings from the literature. First, prior research has shown that ensemble error metrics, such as the root mean squared error against reference data, decrease markedly as the ensemble grows and tend to stabilize once roughly five models are included, a behaviour observed consistently across different study settings (Herger et al., 2018; Milinski et al., 2020). Second, (Deser et al. 2012) demonstrated that in tropical regions, three to six ensemble members are sufficient to capture the climate dynamics of variables such as temperature and precipitation. Third, restricting the ensemble size helps limit redundancy among GCMs that share common structural components (Herger et al., 2018). Beyond this threshold, adding more models brings little improvement in skill while increasing computational cost and the risk of introducing redundant information into the ensemble. We identified the best-performed CMIP6 models among all 10 CMIP6 GCMs using a ranking score. Five criteria were chosen for evaluation: the annual mean (mean), interannual coefficient of variation (Cv), Mann-Kendall Z-statistic (Z), Theil-Sen slope estimator (β), and normalized root mean square error (NRMSE). The degree of the alignment between GCM output and reference data was measured as follows:

$$Z = |Z_i - Z_o| \tag{1}$$

where Z_i represents the value of the i-th model evaluation metric, and Z_o the corresponding reference value. The rank scores are calculated as follows:

$$RS = \left(1 - \frac{X_i - X_{min}}{X_{max} - X_{min}}\right) \times 10 \tag{2}$$

where X_i is the statistic of X of the i-th model; X_{max} and X_{min} are the maximum and minimum values of the statistic X across models.

The best-performed CMIP6 GCMs models for each variable were selected based on the average rank score (RS), finally the best-performed CMIP6 GCMs models for the two variables together were selected based on average score from RS for each model. A typical RS value nearing 10 indicates the top-performing model. This implies that the model consistently demonstrates excellent performance across all criteria, making it a dependable option for simulating precipitation characteristics and conducting hydrologic analysis.

2.3.2. Quantile-Delta-Mapping (QDM) bias correction

The application of GCMs in climate change impact assessment is critical for simulating large-scale climate processes and that is constrained by the inherent systematic biases, particularly in representing local precipitation patterns. Then, is necessary important to correct these biases before performing a reliable study in precipitation patterns evaluation The Quantile Delta Mapping method (Cannon et al., 2015) has gained broad recognition as one of the leading approaches to bias adjustment. Unlike conventional univariate techniques, which target only the mean or variance, QDM corrects biases throughout the full statistical distribution. QDM also takes the change between the modelled data of the control and scenario period into account. The QDM is given as follows; for the historical period, the correction approach followed the standard Quantile Mapping method.

$$Xcor_{s,h}(t) = F_{o,h}^{-1}(F_{s,h}(x_{s,h}(t)) \tag{3}$$

where $x_{s,h}(t)$ represents the simulated value and $Xcor_{s,h}(t)$ is the corrected historical values for time step *t* respectively. $F_{s,h}$ corresponds to the cumulative distribution function (CDF) derived from the historical simulation data and $F_{o,h}^{-1}$ is the inverse CDF of observational data from baseline period. To adjust the simulation of projected period, the bias correction approach follows a two-step. First, the Quantile Mapping (QM) method is used to reduce systematic bias in the simulated data (Equations 4-5). Next, the quantile-dependent variations between the projected and past model outputs are calculated using (Equation 6). These changes are then applied directly to the bias-corrected values as shown in (Equation 7).

$$x_o(t) = F_{s,p}(x_{s,p}(t)) \tag{4}$$

$$x_{ohp}(t) = F_{o,h}^{-1}((x_o(t)) \tag{5}$$

$$\Delta_s(t) = \begin{cases} F_{s,p}^{-1}(x_o(t)) / F_{s,h}^{-1}(x_o(t)), for\ precipitation \\ F_{s,p}^{-1}(x_o(t)) - F_{s,h}^{-1}(x_o(t)), for\ temperature \end{cases} \tag{6}$$

$$x_{proj}(t) = \begin{cases} x_{ohp}(t) \times \Delta_s(t), for\ precipitation \\ x_{ohp}(t) + \Delta_s(t),\ for\ temperature \end{cases} \tag{7}$$

where $x_{s,p}(t)$ and $x_o(t)$ represent the models simulated outputs together with their associated quantile for time step t for the future projection period, $F_{s,p}$ and $F_{s,p}^{-1}$ denote to the cumulative distribution function (CDF) of the model outputs over the projection period, as well as its inverse, respectively. $x_{ohp}(t)$ is an intermediate corrected value for time step t; obtained by projecting the future-period model quantile to the inverse of CDF drawn from historical observations. $\Delta_s(t)$ represents the relative variation between the quantile-matched values from the past and projection periods. Finally, the $x_{proj}(t)$ gives the QDM-corrected model value for the future period. Although QDM is one of the most robust approaches for quantile-dependent bias correction, it relies on the stationarity assumption of the transfer function: biases identified during the historical period are assumed to remain valid in future climate. Furthermore, the reliability of the correction decreases at extreme quantiles (>99 %) where the sample becomes sparse, and the univariate application to precipitation and temperature does not explicitly preserve their bivariate dependence.

2.3.3. Multi-Model Ensemble (MME's)

The weighted average (WA) method is a multimodel ensemble (MME) approach used to combine CMIP6 GCMs models simulations from multiple models by assigning a relative weight to each model based on predefined criteria. In this study the WA method gives weights according to model performance measured by RMSE, models with lower RMSE values receive stronger emphasis, thereby improving the robustness and reliability of the ensemble estimate. The WA is given as follows:

$$RMSE_i = \sqrt{\frac{1}{n} \sum_{i=1}^{n} (S_i - O_i)} \tag{8}$$

$$\omega_i = \frac{1/RMSE_i}{\sum_{i=1}^{N} (1/RMSE_i)} \tag{9}$$

$$WA = \sum_{i=1}^{N} \omega_i . S_i \tag{10}$$

where $RMSE_i$ represents the root mean square error between i-th model outputs and the observed data; S_i denotes the model outputs for time step t and O_i is the observed data for baseline period at time t, respectively; ω_i is the weight given to the i-th model; and WA represents the weighted ensemble output at time t

- **Extreme precipitation indices**

To provide a meaningful evaluation of projected changes in extreme precipitation, four indices drawn from the Expert Team on Climate Change Detection, Monitoring and Indices (ETCCDI) (Zhang et al., 2011) are retained in this study (Table 2).

Table 2. List of precipitation indices used

Indices	Indicator name	Definitions	Units
RX1day	Max 1-day precipitation	Monthly maximum 1-day precipitation	mm
SDII	Simple daily intensity index	Annual total precipitation divided by the number of wet days (defined as PRCPTOT ≥1.0 mm) in the year	mm/day
PRCPTOT	Annual total wet day rainfall	Annual total PRCP in wet days (PR ≥ 1 mm)	mm
R20	Number of very heavy rainfall days	Annual count of days when PRCP ≥ 20 mm	day

2.3.4. Trend analysis

- **Mann-Kendall Trend analysis**

In this work we performed the precipitation trend analysis using the Modified Mann Kendall (MMK) (Hamed & Ramachandra Rao, 1998) method. The test is nonparametric and rank-based; it evaluates the trend behavior of a given time series under the null hypothesis of no trend. The MMK statistic (S) is given as:

$$S = \sum_{i=1}^{n-1} \sum_{j=i+1}^{n} sgn(Y_j - Y_i) \tag{11}$$

where, Y_j and Y_i are the rank of jth and ith observations, respectively out of the total number of observations and the function $sgn(Y_j - Y_i)$ is calculated as:

$$sgn(Y_j - Y_i) = \begin{cases} 1 & if\ (Y_j - Y_i) > 0 \\ 0 & if\ (Y_j - Y_i) = 0 \\ -1 & if\ (Y_j - Y_i) < 0 \end{cases} \tag{12}$$

The $var\ (S)$ for the Z-statistics was computed as follows:

$$var\ (S) = \frac{n(n-1)(2n+5) - \sum_{i=1}^{m} t_i(t_i-1)(2t_i+5)}{18} \tag{13}$$

here n refers to the total count of available observations, m is the number of ties and t_i denotes the number of ties of extent i. S follows an approximate normal distribution with mean E(S) = 0. Then Z_s is calculated as follows:

$$Z_s = \begin{cases} \frac{S-1}{\sqrt{var(S)}}, & if \quad S > 0 \\ 0, & if \quad S = 0 \\ \frac{S+1}{\sqrt{var(S)}}, & if \quad S < 0 \end{cases} \tag{14}$$

When Zs is positive, we denote increasing trend, while negative values indicate the decreasing trend.

- Sen's slope estimation

Developed by (Sen 1968), the Sen this non-parametric approach serves to quantify the magnitude of trends within a time series. Its robustness against outliers makes it well-suited for capturing linear trends in irregular datasets. For this reason, it has seen extensive application in hydro-climatic research(Ahmed et al., 2022; Konate et al., 2023; Koubodana et al., 2019; M'Po et al., 2017). In this method firstly, the slopes (T_i) of time-series data are calculated as:

$$T_i = \frac{x_j - x_k}{j-k} \tag{15}$$

where i is the number of data (N) in the data series, x_j and x_k are data values at time j and k ($j > k$) respectively. T_i estimation is the median of N values, $T_i$is Sen's estimator which is computed as:

$$\beta = \begin{cases} T_{\frac{N+1}{2}} \; if \; N \; is \; odd \\ \frac{T_{\frac{N}{2}} + T_{\frac{N+2}{2}}}{2} \; if \; N \; is \; even \end{cases} \tag{16}$$

- Innovative Trend Analysis (ITA)

Innovative Trend Analysis (ITA) is a visual method developed to detect monotonic trends within hydro-meteorological time series (Şen, 2011). The dataset is first split into two equal halves. Each half is then ranked by ascending order. The first is placed on the x-axis, while the second is positioned on the y-axis of a Cartesian coordinate system. A reference line is drawn across the resulting scatter plot. This line shows whether a monotonic trend is present or not. Points located above the 1:1 line, in the upper triangle, indicate an increasing trend, while those below it, in the lower triangle, show a decreasing trend. Points clustering near the 1:1 line suggest a flat trend in the series (Şen, 2011). Beyond overall direction, the ITA graph also allows different trend behaviors to be read at various sub-intervals within the dataset. The slope is then calculated following the formula of Şen (Şen, 2015):

$$S_{ITA} = \frac{2(\bar{x}_j - \bar{x}_i)}{n} \tag{17}$$

where $\bar{x}_j$ and $\bar{x}_i$ denote the arithmetic averages of the first and second halves of the x sequence respectively, n being the number of data points. S_{ITA} denotes the ITA slope.

The trend indicator is calculated as follows:

$$D = \frac{1}{N} \sum_{i=1}^{N} \frac{10(x_j - x_i)}{\bar{x}} \tag{18}$$

N is the length of each subseries, x_j and x_i are values of consecutive subseries, and $\bar{x}$ is the mean of the first half subseries. A positive value of D indicates an increasing trend, whereas a negative value indicates a decreasing trend. To compare ITA with MMK test method, we multiplied D by 10 for as stated by (Wu et al. 2017). The joint use of the Modified Mann-Kendall test and ITA follows a cross-validation logic: MMK quantifies the statistical significance of an overall monotonic trend, while ITA, through its graphical decomposition into low, medium, and high values, allows the detection of trends specific to different parts of the distribution particularly useful for extreme indices whose upper tail may evolve differently from the body of the distribution. When both methods agree, the robustness of the result is reinforced; when they diverge, it signals a complex or non-monotonic trend that a single test could miss.

- Spatial patterns of rainfall changes

The rate of change in mean precipitation indices was calculated to evaluate how climate change affects extreme precipitation indices. Examining its spatial distribution makes it possible to compare projected shifts under the SSP2-4.5 and SSP5-8.5 scenarios against the baseline period, as expressed below:

$$Rate = \frac{Z_{proj} - Z_{ref}}{Z_{ref}} \times 100 \tag{19}$$

where Rate denotes the rate of variation between reference period and projected period, Z_{proj} denotes the future projection of extreme precipitation indices bias corrected under SSP2-4.5 and SSP5-8.5 scenario over the period of (2030-2060) and Z_{ref} represents extreme precipitation indices from the reference period.

3. Results

3.1. Selection and analysis of CMIP6 GCMs

To assess the ability of 10 GCMs for reproducing observed precipitation and temperature data over Mono River Basin, five evaluation metrics were calculated for the period of 1985–2014 (Table 3). The result show that all CMIP6 GCMs models tend to underestimate the annual mean precipitation (1208.88 mm) in varying degrees. Most models reproduce the mean annual rainfall reasonably well, with simulated values ranging from 1157.74 mm (MIROC6) to 1191.92 mm (ACCESS-CM2). ACCESS-CM2, CNRM-CM6-1 and CNRM-ESM2-1 show the closest agreement with observed mean rainfall. In terms of interannual variability, most models exhibit coefficients of variation (Cv) for annual basin precipitation that closely approximate the value from the reference data (11.40 %), with MPI-ESM1-2-HR showing the closest match (12.50 %). During the baseline period, annual precipitation of observed data shows a statistically increasing trend ($|Z| > 0.46$), while 7 models also simulate increasing trends ($Z, \beta > 0$), with MPI-ESM1-2-LR exhibiting the strongest ($Z = 1.62$). The NRMSE values range from 1.82 to 1.97. ACCESS-CM2 and MPI-ESM1-2-LR exhibit relatively lower NRMSE values, while TaiESM1 and NorESM2-MM show higher errors. The same evaluation metrics were evaluated for temperature for all of our 10 CMIP6 GCMs for the historical period, as shown in (Table 4). Over the period, the annual mean temperature in the Mono River Basin is 26.19 °C, while the model MPI–ESM1-2-HR provides the closest estimation (26.87 °C). Among all models, CNRM-ESM2-1 produced a Cv of 1.14 the value nearest to the reference dataset. Across all CMIP6 GCMs, annual mean temperature consistently trended upward throughout the reference period. NRMSE values fell between 0.06 and 0.074 and pointed out that all models achieving values below 0.5. Per-model scores for each evaluation metric are shown in Figures 2a and 2b for precipitation and temperature respectively.

Table 3. Performance evaluation of CMIP6 GCMs for simulated precipitation.

model	Mean [mm]	CV [%]	Z	β	NRMSE
Observed	1208.88	11.76	0.46	1.80	-
ACCESS-CM2	1191.92	6.32	0.2	0.05	1.82
BCC-CSM2-MR	1160.89	8.25	-0.25	-0.66	1.84
CNRM-CM6-1	1190.10	8.60	0.93	2.62	1.89
CNRM-ESM2-1	1191.24	9.40	1.25	4.11	1.89
TaiESM1	1179.79	17.18	0.2	-0.03	1.97
GFDL-ESM4	1159.68	10.93	1.15	2.75	1.89
MIROC6	1157.74	8.25	-2.34	-3.09	1.91
MPI-ESM1-2-HR	1186.42	12.50	1.36	4.34	1.88
MPI-ESM1-2-LR	1181.86	8.51	1.62	2.54	1.83
NorESM2-MM	1181.73	16.46	-0.14	-0.75	1.94

Table 4. Performance evaluation of CMIP6 GCMs for simulated temperature.

model	Mean [°C]	CV [%]	Z	β	NRMSE
Observed	26.19	1.1	3.67	0.02	-
ACCESS-CM2	27.05	1.82	2.93	0.03	0.07
BCC-CSM2-MR	26.98	1.2	4	0.03	0.06
CNRM-CM6-1	26.99	1.26	3.28	0.02	0.06
CNRM-ESM2-1	26.9	1.14	2.6	0.02	0.06
TaiESM1	26.93	1.98	3.18	0.05	0.06
GFDL-ESM4	27.07	2.13	9.39	0.05	0.07
MIROC6	26.92	1.59	3.1	0.03	0.06
MPI-ESM1-2-HR	26.87	1.89	0.5	0.01	0.07
MPI-ESM1-2-LR	26.88	1.31	0.04	0.01	0.07
NorESM2-MM	26.94	3.1	2.16	0.05	0.07

In summary, while most of CMIP6 GCMs models reasonably capture the mean annual rainfall and temperature over the Mono River Basin, their performance varies significantly in terms of variability, bias, and error structure. None of the models consistently outperforms others on every metric assessed, highlighting the relevance of a multi-model ensemble approach to reduce individual model uncertainties. According on the average rank scores for precipitation and temperature simulation across the 10 GCMs (Figure 2c), five models with relatively superior performance in simulating precipitation and temperature conditions over the Mono River Basin were selected: CNRM-CM6-1, MPI-ESM1-2-HR, MPI-ESM1-2-LR, CNRM-ESM2-1, BCC-CSM2-MR.

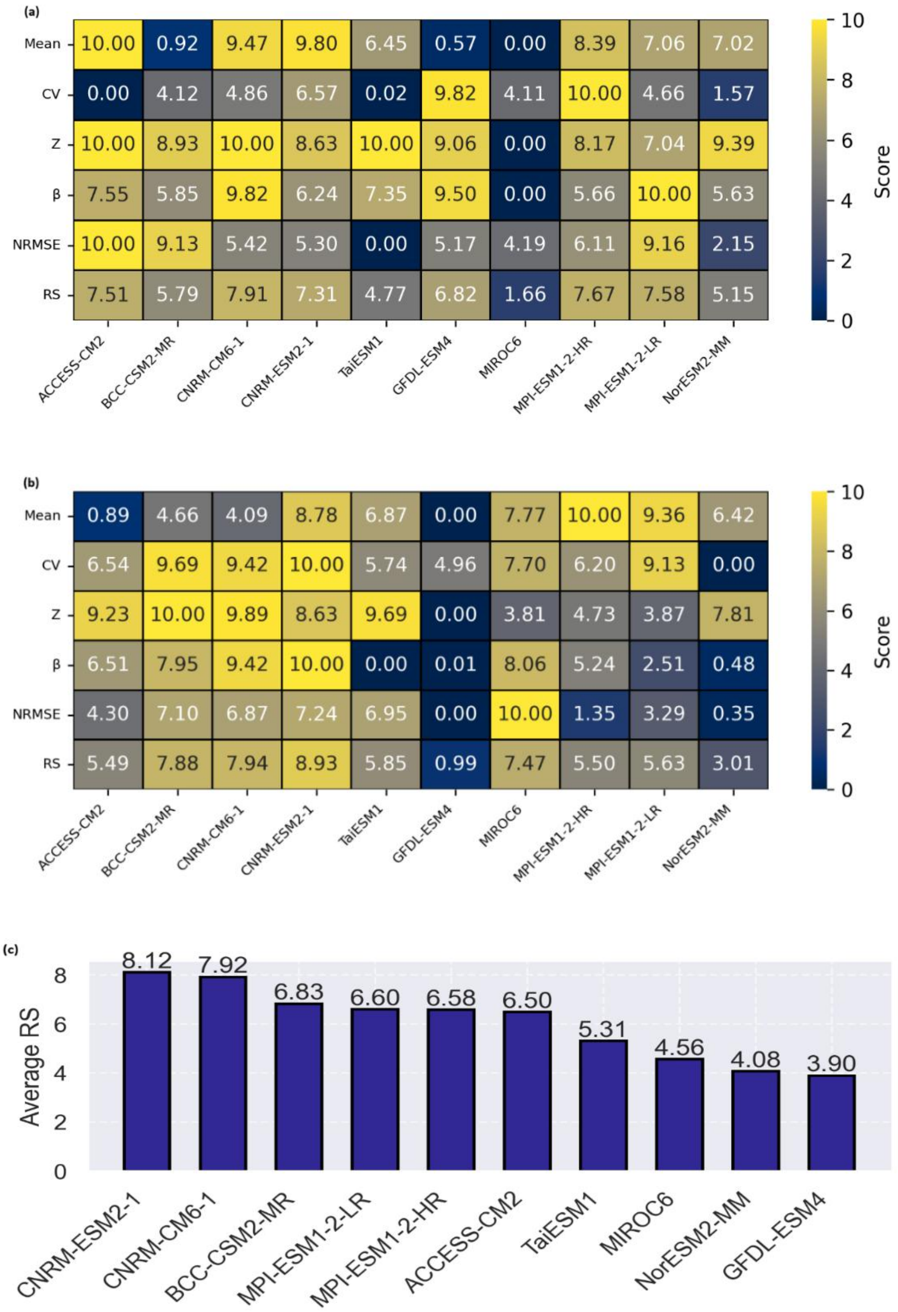

Figure 2. Ranking of 10 CMIP6 GCMs based on their performance in reproducing precipitation (a), temperature (b), and their combined score (c) over the Mono River Basin for the baseline period (1985–2014). Models with higher scores performed better across both variables overall.

3.2. Evaluation of multi-model ensemble methods

The performance of output of the five selected CMIP6 climate models bias-corrected was evaluated using RMSE, R^2, NSE, and KGE metrics as shown in (Table 5). For the precipitation data, individual models show moderate to good skill, indicating an acceptable representation of observed rainfall variability. Among them, MPI-ESM1-2-LR and CNRM-ESM2-1 exhibit relatively good performance, particularly in terms of lower RMSE and higher efficiency scores. The CNRM-ESM2-1 model achieves an RMSE of 50.23, an R^2 of 0.65, an NSE of 0.62 and a KGE of 0.74, indicating a good ability to reproduce the variability of observed precipitation. Similarly, MPI-ESM1-2-LR has an RMSE of 50.76, an R^2 of 0.65, an NSE of 0.61 and a KGE of 0.75. However, the Weighted Average (WA) multi-model ensemble approach demonstrates the highest overall performance, achieving the lowest RMSE (41.91 mm) and the highest R^2 (0.76), NSE (0.74), and KGE (0.76). For the temperature simulations, Among the individual models, CNRM-CM6-1 show best result, with the highest R^2 (0.74), NSE (0.73), and KGE (0.84), and a low RMSE (0.84). BCC-CSM2-MR and CNRM-ESM2-1 also exhibit good agreement with observations over the baseline period. In contrast, MPI-ESM1-2-HR performs worst, with higher errors and lower skill scores, while MPI-ESM1-2-LR shows intermediate results. The weighted average method (WA) outperforms all individual models, yielding the lowest RMSE (0.79) and the highest R^2 (0.79), NSE (0.77), and KGE (0.85), highlighting the added value of the ensemble approach. Also, WA results for precipitation and temperature were assessed against the reference data (Figure 5). The monthly rainfall time series highlights a strong agreement between the observed precipitation and the weighted average (WA) simulation over Mono River Basin for the study period. Both series clearly reproduce the seasonal cycle, with well-defined wet and dry phases recurring consistently from year to year. In the majority of months, WA simulations agreed reasonably well with the reference dataset, while slightly smoothing extreme rainfall peaks. The WA approach successfully captures the seasonal cycle, with consistent warm and cool phases throughout the years. Overall, the simulations closely match the reference data, with only slight smoothing of extreme temperature values.

Table 5. Performance assessment of bias-corrected GCMs and the Weighted Average approach in reproducing precipitation and temperature over the baseline period (1985–2014).

model	**Precipitation**				**Temperature**			
	RMSE	**R^2**	**NSE**	**KGE**	**RMSE**	**R^2**	**NSE**	**KGE**
BCC-CSM2-MR	53.14	0.61	0.58	0.72	0.88	0.72	0.70	0.81
CNRM-CM6-1	51.55	0.63	0.6	0.73	0.84	0.74	0.73	0.84
CNRM-ESM2-1	50.23	0.65	0.62	0.74	0.86	0.73	0.72	0.83
MPI-ESM1-2-HR	56.01	0.58	0.53	0.72	1.23	0.49	0.44	0.69
MPI-ESM1-2-LR	50.76	0.65	0.61	0.75	1.1	0.57	0.54	0.73
WA	41.91	0.76	0.74	0.76	0.79	0.79	0.77	0.85

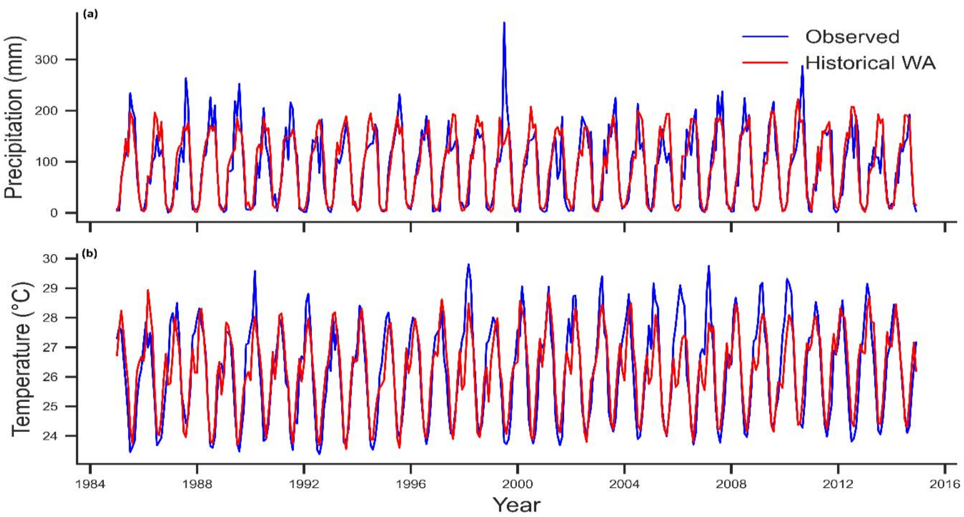

Figure 3. Skill of the WA multi-model ensemble in capturing seasonal precipitation (a) and temperature (b) over the baseline period (1985–2014).

3.3. Ensemble projection and seasonal analysis of the MME

Figure 4a compares the monthly rainfall cycle for the historical baseline period (1985–2014) to the future projection period (2030–2060) under SSP2-4.5 and SSP5-8.5 scenarios. The first three panels (a-c) represent the decadal evolution (2030-2039, 2040-2049, and 2050-2059), while the fourth panel shows the monthly rainfall distribution over the entire 2030–2060 period. The result demonstrates that, the seasonal rainfall pattern of projected period remains well defined across all periods following seasonal phases in the baseline, and shows the main rainy season extending roughly from April to October and peak rainfall occurring in August-September. However, both future scenarios indicate a gradual increase in monthly rainfall during the wet season, particularly in August and September. This increase is more pronounced under the SSP5-8.5 scenario. Changes during the dry season (November-February) remain limited, with rainfall totals staying relatively low and close to historical baseline value. The mean monthly rainfall over 2030-2060 confirms this general tendency, showing a moderate increase under SSP2-4.5 and a marked intensification under SSP5-8.5 during peak rainfall months. Figure 4b shows that mean monthly rainfall is projected to intensify more sharply relative to the historical baseline (1985–2014), especially under SSP5-8.5. Under SSP2-4.5, rainfall decreases are observed mainly during the dry season and early rainy season (December to July), with the strongest reductions occurring for December-April with loss of -20 – 3 % (10 - 15 mm/month). In contrast, rainfall increases appear from August to November, with a marked peak in November gaining 7-20% (10 - 25 mm/month). Under SSP5-8.5, the magnitude of change is more pronounced. Rainfall is expected to drop considerably over the January-April period, reaching stronger negative anomalies than under SSP2-4.5; -28 – 8 % (15 - 35 mm/month). From August onward, significant increases are observed, with the highest rise occurring in November 8-28 % (up to 50 mm/month). The wet-season intensification is clearly stronger under SSP5-8.5 compared to SSP2-4.5.

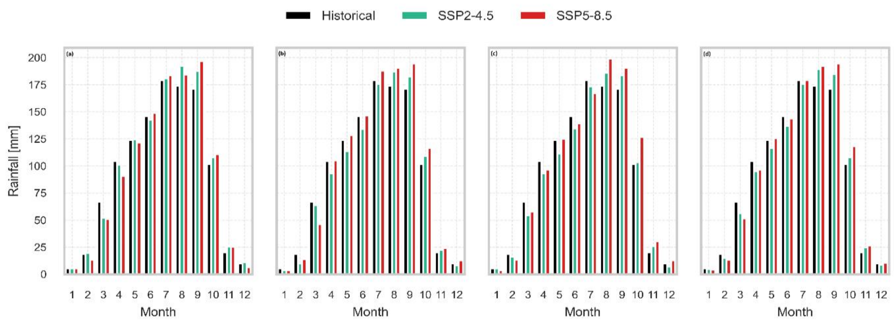

Figure 4a. Monthly mean rainfall over the baseline period (1985-2014) and the projected rainfall 2030–2039 (a), 2040–2049 (b), 2050-2059 (c) and 2030-2060 (d) under the SSP2-4.5 and SSP5-8.5 scenarios over the Mono River Basin.

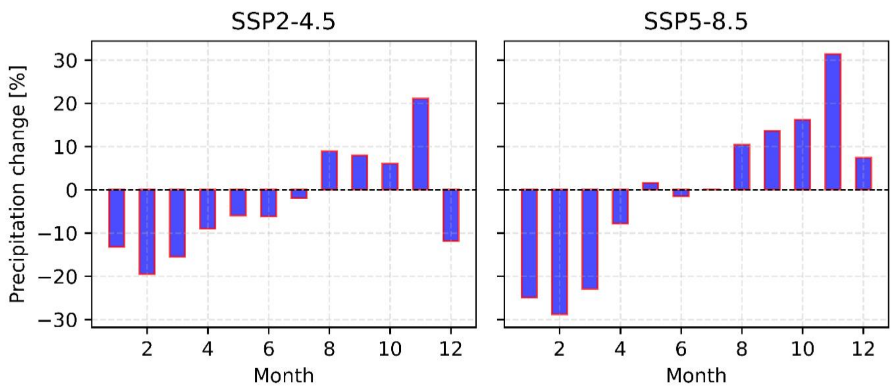

Figure 4b. Projected Changes in Mean Monthly Rainfall Relative to the 1985–2014 Baseline under SSP2-4.5 and SSP5-8.5 Scenarios during 2030-2060 period.

3.4. Temporal variability in extreme precipitation indices

Figure 5 illustrates trend analysis of four projected extreme precipitation indices (Rx1day, SDII, PRCPTOT, and R20) under SSP2-4.5 (a-d) and SSP5-8.5 (e-h) using ITA graphical method. The summarized results can be found in Table 6 Both the MMK test and ITA methods highlighted the same trend for the all-extreme precipitation indices for the two scenarios over MRB, except for PRCPTOT in SSP5-8-5. Indeed, the 90% and 95% confidence bands plotted around the 1:1 line provide a graphical test of trend significance complementary to the MMK results in Table 6. Points falling outside the 95% band indicate trends that are statistically significant at the 5% level, points between the 90% and 95% bands correspond to weaker but still meaningful signals, and points contained within the 90% band denote changes that cannot be distinguished from natural variability. Under SSP2-4.5 (panels a–d), most stations cluster tightly along the 1:1 line and remain within the 90% band for Rx1day, SDII, and PRCPTOT, indicating that the projected changes between the first half (2030–2044) and the second half (2045–2060) of the period are not statistically distinguishable from no-trend behaviour. R20 (panel d) shows a wider spread, with several stations falling below the 95% band consistent with the significant decreasing trends flagged by the MMK test in Table 6. Under SSP5-8.5 (panels e–h), the dispersion increases markedly. For Rx1day (panel e) and R20 (panel h), a non-negligible fraction of stations lies outside the 95% band, predominantly below the 1:1 line, which corroborates the significant negative trends identified by MMK. SDII (panel f) and PRCPTOT (panel g) display a larger number of points crossing the 90% band, suggesting emerging but weaker signals under the high-emission scenario. Overall, the joint reading of the ITA confidence bands and the MMK results indicates that trend significance is scenario-dependent and index-dependent: SSP5-8.5 amplifies the proportion of stations exhibiting statistically detectable changes, particularly for intensity-related indices.

Table 6. Trend analysis of extreme precipitation indices under SSP2.4-5 and SSP5.8-5 scenarios for the period of (2030-2060) using MMK test and ITA

	Z statistics	**Sen's Slope**	**MMK tau**	**ITD**	**ITA Slope**
			SSP2.4-5		
Rx1day	1.292*	0.041	0.166	Inc	0.088
SDII	-1.82	-0.08	-0.23	Dec	-0.07
PRCPTOT	-2.344*	-2.577	-0.299	Dec	-3.682
R20	-0.002	-0.002	-0.001	Dec	-0.034
			SSP5.8-5		
Rx1day	1.87*	0.1	0.239	Inc	0.165
SDII	1.099*	0.005	0.135	Inc	0.06
PRCPTOT	0.544	1.064	0.071	No trend	0.125
R20	3.240*	0.154	0.241	Inc	0.124

* Indicates trends statistically significant at the 95% confidence level. Both Sen's slope and ITA slope are expressed in mm.yr^{-1}. ITD stands for Innovative Trend Detection. (Inc) and (Dec) refer to increasing and decreasing trends as identified by the ITA. The MMK test assesses the statistical significance of Z-scores; MMK Tau indicates trend direction positive, negative, or absent.

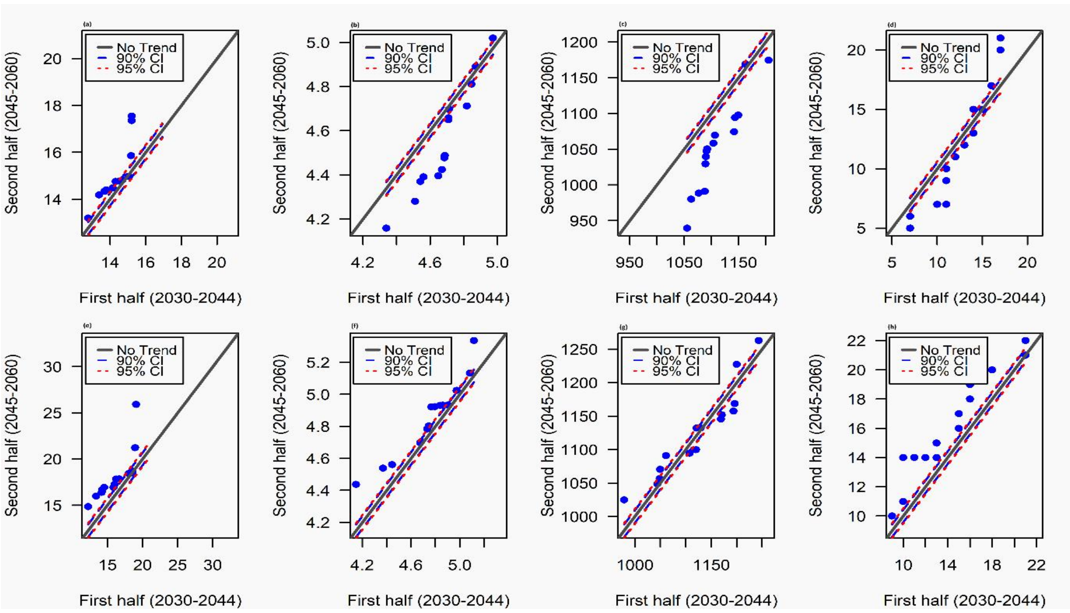

Figure 5. Trend analysis of four projected extreme precipitation indices (Rx1day, SDII, PRCPTOT, and R20) under SSP2-4.5 (a-d) and SSP5-8.5 (e-h) using ITA graphical method for period of 2030-2060.

3.5. Spatial variability and trend of extreme precipitation indices

Figure 6 presents the spatial distribution of four indices across MRB during the baseline period, with observed data (a-d) and the weighted average (WA) of the GCM outputs (e-h). The analysis of the spatial variability of rainfall indices highlights marked geographical contrasts over the basin. For Rx1day, higher values are observed in the central and northern parts of the basin (up to 40 mm), while lower magnitudes occur toward the southern; the WA simulation reproduces this spatial gradient reasonably well, although with slightly smoother patterns and moderately higher values in some locations with high value around 60 mm. A similar north-south contrast is evident for SDII, where stronger rainfall intensity is observed in the northern sector up to 10 mm/day for observed data; this gradient is generally captured by the WA ensemble despite some spatial smoothing and minor differences in magnitude. Regarding PRCPTOT, the observed annual rainfall shows a clear spatial gradient, with higher totals in the central and northern zones and lower amounts in the south, and this large-scale pattern is successfully reproduced by the WA simulation, though local extremes appear attenuated. Finally, R20 values are higher in the northern and central areas and lower in the southern basin, and the WA ensemble adequately represents this spatial structure, with slight overestimation in certain grid cells. Overall, these results indicate that the WA method effectively captures the spatial structure of extreme precipitation indices while smoothing local maxima.

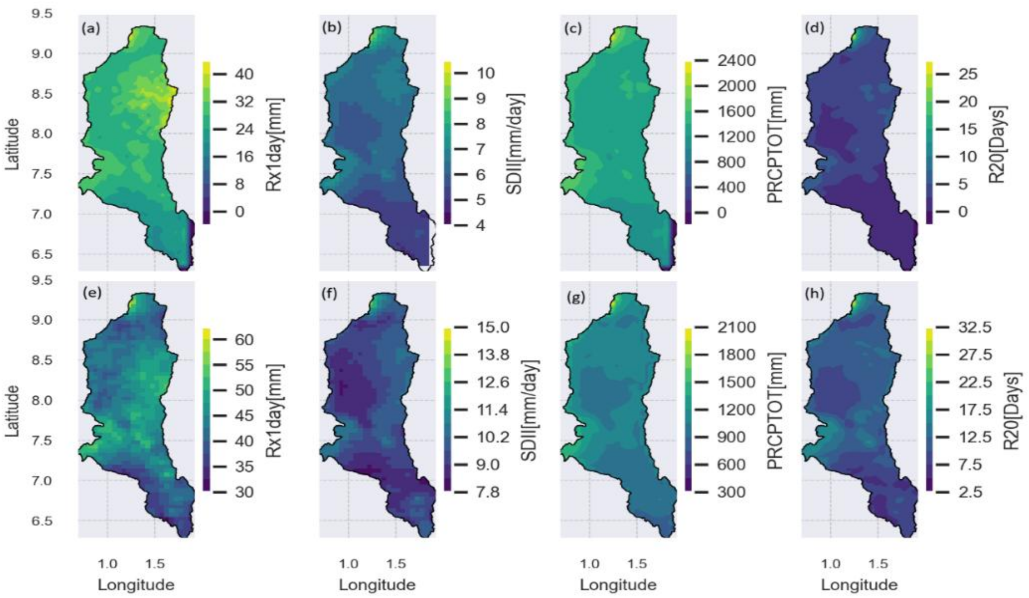

Figure 6. Spatial distribution of recent precipitation indices for baseline period 1985-2014 for reference data (a-d) and for weighted average (e-h)

Figure 7 illustrates the projected spatial changes in four precipitation extreme indices (Rx1day, SDII, PRCPTOT, and R20) for the period 2030–2060 relative to the baseline period, under SSP2-4.5 (a-d) and SSP5-8.5 (e-h). Under SSP245, a general decrease in extreme rainfall intensity is observed across the Mono River Basin. Rx1day shows predominantly negative changes, particularly in the southern and central areas, indicating a reduction in maximum 1-day rainfall events. SDII also exhibits widespread negative anomalies, suggesting a decline in rainfall intensity. In contrast, PRCPTOT displays moderate positive changes over large portions of the basin indicating a slight increase in total annual rainfall despite reduced intensity indices, while display negative change along the central western and south western parts of the catchment. R20 shows limited spatial changes, with slight decreases in most areas. Under SSP5-8.5, the magnitude of changes becomes more pronounced. Rx1day and SDII show stronger negative signals across nearly the entire basin, indicating a potential reduction in rainfall intensity and daily extremes. However, PRCPTOT reveals more substantial increases compared to SSP2-4.5, suggesting that total annual rainfall may rise under the high-emission scenario. Notably, R20 exhibits marked positive changes in several areas, particularly in the central and northern parts, indicating a possible increase in the frequency of heavy rainfall days despite reductions in maximum daily intensity. As a result, multi-model ensemble approaches are widely used to reduce uncertainty and provide more reliable estimates of future climate conditions.

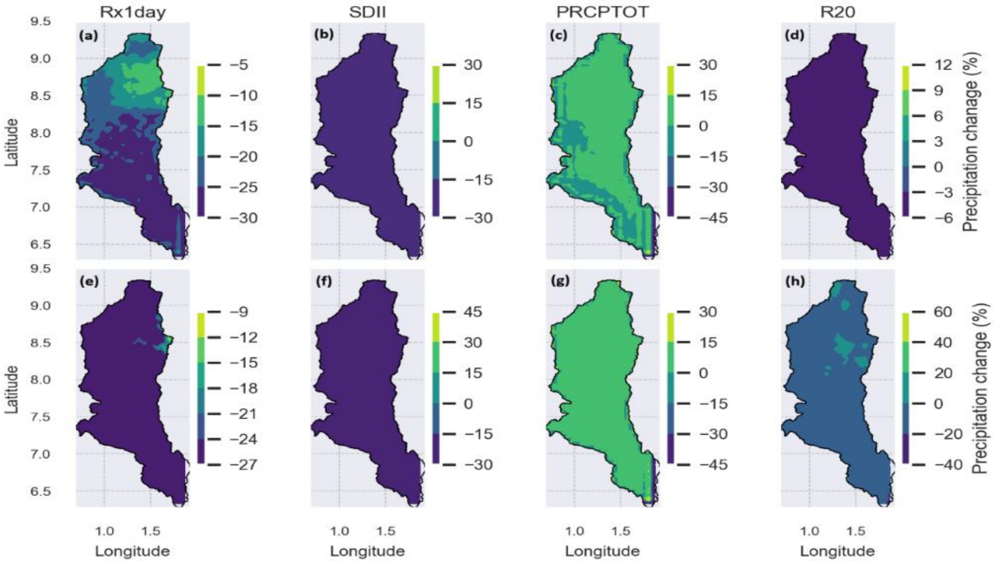

Figure 7. Spatial distribution of change in projected extreme precipitation indices under SSP2-4.5 (a-d) and SSP5-8.5 (e-h) scenarios during the period of 2030-2060.

The Spatial analysis of future extreme precipitation indices trends based on the Mann-Kendall test (Z values) under the SSP2-4.5 and SSP5-8.5 scenarios reveals a widespread drying signal over the Mono River Basin (Figure 8), although spatially modulated according to the intensity of radiative forcing. In both scenarios, the Rx1day trended upward across the basin, with the most pronounced gains recorded in the southern areas, while the northern region exhibits slight decreases or near-neutral changes and exhibits widespread increases over the basin, with stronger intensification in central and southern parts of the basin. SDII shows a marked and spatially consistent increase in rainfall intensity, particularly in the southern half of the basin and this become developed and amplified under SSP5-8.5. The PRCPTOT index exhibits predominantly positive Z-values over the basin, with the highest values under SSP2-4.5 in south parts of basin and particularly concentrated in the north-central parts of the basin under SSP5-8.5. R20 indicates an increase in heavy rainfall days across several parts of the basin, particularly in the south, suggesting a higher frequency of intense precipitation extreme under SSP2-4.5 and that become robust and pronounced under SSP5-8.5, especially in the central and southern of the basin, implying a significant rise in extreme rainfall occurrence. The stronger responses of these indices under SSP5-8.5 emphasize the necessity of climate mitigation efforts to limit the amplification of extreme hydrological events. Under both SSP2-4.5 and SSP5-8.5, the consistently high value of positive Z-statistics indicates a marked rise in hydrological variability. This calls for large-scale adaptive watershed management.

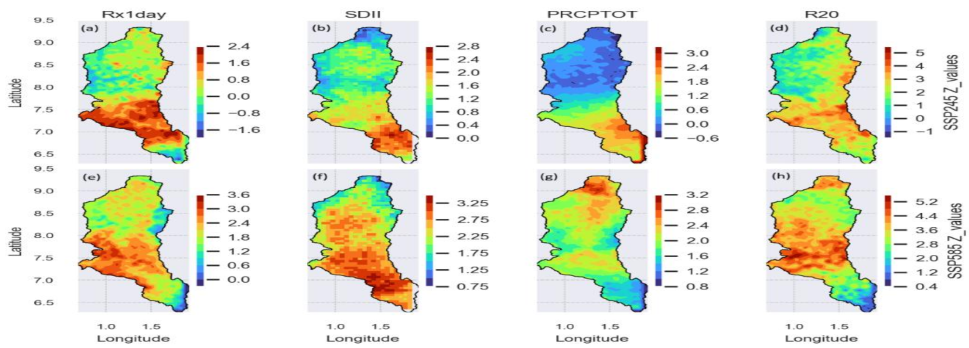

Figure 8. Spatial distribution of future Z value of extreme precipitation indices under SSP2-4.5 (a-d) and SSP5-8..5 (e-h).

4. Discussion

This work provides a comprehensive analysis of the future spatiotemporal evolution of extreme precipitation indices in Mono River Basin. Utilizing a multimodel approach of CMIP6 models for future climate data and CHIRPS precipitation data as reference, the research highlights the future spatiotemporal variability and trends of extreme precipitation indices in the MRB under multiple emission scenarios. The robust methodologies employed, including selection of CMIP6 GCM, bias adjustment and multimodel ensemble using weighted average of selected climate models and spatiotemporal variability and trends analysis, ensure the reliability and completeness of the analysis, establishing a solid foundation for understanding climate variability in the study area. By applying five evaluation criteria including annual mean (mean), interannual variability (coefficient of variation, Cv), Mann-Kendall Z-statistic (Z), Theil-Sen slope (β) and normalized root mean square error (NRMSE) for assessing the performance of CMIP6 models compared to CHIRPS precipitation data as reference data, the result show that CMIP6 models underestimate the annual mean precipitation compared with CHIRPS data. However, for the annual mean precipitation we got 1208.88 mm for observation data. These findings are consistent with those of (Amoussou et al. 2020) and (Gandomé et al. 2021) who pointed out that the annual mean precipitation is between 1100 mm and 1300 mm per year in MRB. (Klutse et al. 2021) and (Gandomé et al. 2021) analyze the spatiotemporal change in precipitation in West Africa using CMIP6 dataset and reported that in West Africa, some CMIP6 models performed well when using for precipitation analysis than order and vice-versa for temperature analysis. Therefore, the selection of CMIP6 models should depend on the intended application. For climate analysis, this selection should consider the combined performance of our two variables, precipitation and temperature; the same authors pointed out that most of CMIP6 climate models underestimate the annual mean precipitation compared with CHIRPS observation. These findings are in agreement with the current study, which shows that all of CMIP6 models underestimate annual rainfall and some models performed well in precipitation analysis than temperature analysis. The results of multimodel approach indicate that the weighted average (WA) method effectively captures the spatiotemporal structure of extreme precipitation indices while smoothing local maxima. These finding are consistent with those of (Diatta et al. 2020), (Amoussou et al. 2020) and (Lawin et al. 2019), who reported that the spatial structures of extreme rainfall indices in the Mono River Basin show higher values in the central and north and lower values in the south. This evidence is further supported by (Mahe et al. 2013) and (Sidibe et al. 2020), who reported that in West Africa, the concurrent decrease in SDII and Rx1day under SSP2-4.5, despite a slight increase in PRCPTOT, physically reflects a redistribution of rainfall toward more frequent but less intense events. Three mechanisms can account for this signature: (i) the projected northward shift of the Intertropical Convergence Zone (ITCZ), which lengthens the rainy season in the coastal sector without intensifying its peaks (Sylla et al., 2015; Klutse et al., 2021); (ii) the increase in atmospheric water vapor consistent with the Clausius-Clapeyron relation, which under moderate forcing favors diffuse rainfall rather than extreme convection; and (iii) a partial stabilization of the troposphere that limits the formation of very intense convective cells. Conversely, under SSP5-8.5, the simultaneous increase of all four indices reflects the crossing of non-linear warming thresholds beyond which deep convection becomes more vigorous, in agreement with the conclusions of Nana et al. (2021) for West Africa. The ability of the Weighted Average (WA) of climate models to reproduce these structural gradients is consistent with the conclusions of (Sylla et al. 2015) on the robustness of multi-model projections for West African rainfall extremes. For the annual mean precipitation and temperature, the overall findings are an increasing trend and that are in agreement with those of (Akinsanola et al. 2015) and (Lawin et al. 2019), who reported the increasing trend in annual mean precipitation and temperature for most of CORDEX regional climate models. (Gandomé et al. 2021) pointed out the same increasing trend in annual mean precipitation and temperature with CMIP6 climate models for most region of West Africa. The positive spatiotemporal trends of SDII and PRCPTOT under SSP5-8.5 observed in the MRB are consistent with regional analyses by Nana et al. (2021) showing an intensification of daily rainfall intensity and an increase in annual rainfall accumulation in certain regions of West Africa, particularly in savannah regions that could lead to local flooding. The same author reported that, the increase in the number of days with precipitation ≥ 20 mm (R20) in the MRB is consistent with trends observed in West Africa, where heavy precipitation indices show a gradual increase towards southern regions. These results align with those of (Konate et al. 2023) and (M'Po et al. 2017), who evaluate the change in extreme precipitation indices using CORDEX regional climate models and reported that the increasing rate of extreme precipitation indices is higher in high emissions scenarios for most regions of west Africa. However, (Sylla et al. 2015) reported that future changes in extreme precipitation indices over west Africa are evident but exhibit substantial variability across climate models. This inter-model spread reflects the uncertainty inherent in future climate projections. As a result, multi-model ensemble approaches are widely used to reduce uncertainty and provide more reliable estimates of future climate conditions. Detecting extreme precipitation indices with notable directional trends opens practical pathways for water resource management, flood risk assessment, and agricultural planning. These findings are relevant both to the Mono River Basin and to the wider West African context. The results obtained globally in this study should be interpreted in light of the uncertainties inherent to the climate modeling chain, as a cascade combining scenario uncertainty, model response, internal variability, and regional biases. The inverse-RMSE weighting adopted in our study is consistent with performance-based weighting approaches (Qin Ju et al., 2025), which have proven more reliable than arithmetic averaging, while acknowledging that the non-independence of GCMs (Nana et al., 2021) may introduce residual correlation in the ensemble. Our results, which show a spatial intensification of rainfall extremes in the southern MRB under SSP5-8.5, are consistent at a broader scale with the findings of (Gandomé et al. 2021), Ayugi et al. (2021), and (Almazroui et al. 2020) for tropical Africa, confirming that the coastal basins of the Gulf of Guinea constitute a hotspot of vulnerability to hydrological extremes.

Several limitations related to the data used in this study should be acknowledged. Although CHIRPS has been validated over West Africa (Bichet & Diedhiou, 2018), it tends to underestimate orographic precipitation as well as the most intense convective events; this limitation may translate into a slight underestimation of the Rx1day indices, particularly over the more rugged northern part of the basin. Regarding temperature, the reliance on only three synoptic stations restricts the analysis to the basin scale and prevents a finer spatial characterization. In this respect, the future development of a gridded observational temperature product dedicated to West Africa would represent a significant contribution to this type of study.

5. Conclusions

This research evaluated prospective climate scenarios in the MRB by employing a multicriteria decision approach to identify the most effective CMIP6 GCMs. CMIP6 GCMs were ranked based on five statistical criteria (Annual mean, coefficient of variation, Z statistic of Mann Kendall, Sen's slope and normalized root mean squared error). Finally, five CIMP6 GCMs were retained to build an ensemble using weighted average based on RMSE value between observed and simulated data, that is further used to evaluate the spatiotemporal extreme precipitation indices and trend under climate change scenarios SSP2-4.5 and SSP5-8.5. The result shows that ensemble methods proved more reliable than individual CMIP6 GCMs at capturing observed precipitation and temperature variability over the historical period. Future extreme precipitation indices based on the ensemble method show that MMK and ITA methods agreed on projected trends results regarding extreme precipitation indices, decreasing trend for (SDII, PRCPTOT and R20) and increasing trend for Rx1day under SSP2-4.5. Under SSP5-8.5, extreme precipitation indices show increasing trend for (Rx1day, SDII and R20) for two methods. For PRCPTOT, MMK test indicates a very weak upward trend which is not statistically significant at the 95% confidence level, while the ITA revealed the absence of a clear monotonic trend. The spatial analysis of these indices reveals a clear spatial heterogeneity across the Mono River Basin, with stronger increases generally concentrated in the central and southern of MRB whereas the northern region exhibits weaker or mixed trends. Most indices (Rx1day, SDII, PRCPTOT, and R20) show predominantly positive trends, indicating a spatial intensification of rainfall extremes, particularly downstream. Under the high-emission SSP5-8.5, these spatial contrasts become more sharpen, highlighting an increased risk of extreme precipitation and hydrological variability across the basin. Taken together, these findings confirm that multimodel ensembles can meaningfully improve the accuracy of regional climate projections with direct relevance for hydrological impact studies.

Declaration of competing interest
The authors state that there are no competing interests.

Data Availability
The data used in this study are publicly available at the following addresses: (i) CHIRPS v2.0 precipitation data are accessible through the Climate Hazards Center, University of California Santa Barbara (https://www.chc.ucsb.edu/data/chirps); (ii) CMIP6 GCM outputs (daily precipitation and temperature, r1i1p1f1 runs) were downloaded from the Earth System Grid Federation portal (ESGF, https://esgf-node.llnl.gov/search/cmip6) for the historical, ssp245, and ssp585 experiments; (iii) the reference

temperature series come from the National Meteorological Agency of Togo (ANAMET) and are available upon reasonable request from the corresponding author, subject to ANAMET's conditions

Code Availability

All analysis et graphics were performed using python (3.11). Custom scripts are available upon request from the respective author.

References

Ahmed, I. A., Salam, R., Naikoo, M. W., Rahman, A., Praveen, B., Hoai, P. N., Pham, Q. B., Anh, D. T., Tri, D. Q., & Elkhrachy, I. (2022). Evaluating the variability in long-term rainfall over India with advanced statistical techniques. *Acta Geophysica 2022 70:2*, *70*(2), 801–818. https://doi.org/10.1007/S11600-022-00735-5

Akinsanola, A. A., Ogunjobi, K. O., Gbode, I. E., & Ajayi, V. O. (2015). Assessing the Capabilities of Three Regional Climate Models over CORDEX Africa in Simulating West African Summer Monsoon Precipitation. *Advances in Meteorology*, *2015*(1), 935431. https://doi.org/10.1155/2015/935431

Almazroui, M., Saeed, F., Saeed, S., Nazrul Islam, M., Ismail, M., Klutse, N. A. B., & Siddiqui, M. H. (2020). Projected Change in Temperature and Precipitation Over Africa from CMIP6: M. Almazroui et al. *Earth Systems and Environment*, *4*(3), 455-475.

Amoussou, E. (2010). *Variabilité pluviométrique et dynamique hydro-sédimentaire du bassin versant du complexe fluvio-lagunaire Mono-Ahémé-Couffo (Afrique de l'ouest)*. 255. https://doi.org/10.34894/VQ1DJA

Amoussou, E., Awoye, H., Vodounon, H. S. T., Obahoundje, S., Camberlin, P., Diedhiou, A., Kouadio, K., Mahé, G., Houndénou, C., Boko, M., Amoussou, E., Awoye, H., Vodounon, H. S. T., Obahoundje, S., Camberlin, P., Diedhiou, A., Kouadio, K., Mahé, G., Houndénou, C., & Boko, M. (2020). Climate and Extreme Rainfall Events in the Mono River Basin (West Africa): Investigating Future Changes with Regional Climate Models. *Water 2020, Vol. 12*, *12*(3). https://doi.org/10.3390/W12030833

Asare-Nuamah, P. (2021). Climate variability, subsistence agriculture and household food security in rural Ghana. *Heliyon*, *7*(4), e06928. https://doi.org/10.1016/j.heliyon.2021.e06928

Bichet A, Diedhiou A (2018) West African Sahel has become wetter during the last 30 years, but dry spells are shorter and more frequent. Clim Res 75:155-162 https://doi.org/10.3354/cr01515

Cannon, A. J., Sobie, S. R., Murdock, T. Q., Cannon, A. J., Sobie, S. R., & Murdock, T. Q. (2015). Bias Correction of GCM Precipitation by Quantile Mapping: How Well Do Methods Preserve Changes in Quantiles and Extremes? *Journal of Climate*, *28*(17), 6938–6959. https://doi.org/10.1175/JCLI-D-14-00754.1

De Longueville, F., Ozer, P., Gemenne, F., Henry, S., Mertz, O., & Nielsen, J. (2020). Comparing climate change perceptions and meteorological data in rural West Africa to improve the understanding of household decisions to migrate. *Climatic Change 2020 160:1*, *160*(1), 123–141. https://doi.org/10.1007/s10584-020-02704-7

Deser, C., Knutti, R., Solomon, S., & Phillips, A. S. (2012). Communication of the role of natural variability in future North American climate. *Nature Climate Change 2012 2:11*, *2*(11), 775–779. https://doi.org/10.1038/nclimate1562

Diatta, S., Diedhiou, C. W., Dione, D. M., & Sambou, S. (2020). Spatial variation and trend of extreme precipitation in West Africa and teleconnections with remote indices. https://doi.org/10.3390/ATMOS11090999

Dosio, A., Turner, A. G., Tamoffo, A. T., Sylla, M. B., Lennard, C., Jones, R. G., Terray, L., Nikulin, G., & Hewitson, B. (2020). A tale of two futures: contrasting scenarios of future precipitation for West Africa from an ensemble of regional climate models. *Environmental Research Letters*, *15*(6), 064007. https://doi.org/10.1088/1748-9326

Gandomé, Q. M. L. D., Nkrumah, F., Klutse, N. A. B., & Sylla, M. B. (2021). Spatiotemporal Changes in Temperature and Precipitation in West Africa. Part I: Analysis with the CMIP6 Historical Dataset. *Water 2021, Vol. 13*, *13*(24). https://doi.org/10.3390/w13243506

Hamed, K. H., & Ramachandra Rao, A. (1998). A modified Mann-Kendall trend test for autocorrelated data. *Journal of Hydrology*, *204*(1–4), 182–196. https://doi.org/10.1016/S0022-1694(97) 00125-X

Herger, N., Angélil, O., Abramowitz, G., Donat, M., Stone, D., & Lehmann, K. (2018). Calibrating Climate Model Ensembles for Assessing Extremes in a Changing Climate. *Journal of Geophysical Research: Atmospheres*, *123*(11), 5988–6004. https://doi.org/10.1029/2018 JD028549

Klutse, N. A. B., Quagraine, K. A., Nkrumah, F., Quagraine, K. T., Berkoh-Oforiwaa, R., Dzrobi, J. F., & Sylla, M. B. (2021). The Climatic Analysis of Summer Monsoon Extreme Precipitation Events

Over West Africa in CMIP6 Simulations. *Earth Systems and Environment 2021 5:1*, *5*(1), 25–41. https://doi.org/10.1007/s41748-021-00203-y
Konate, D., Didi, S. R., Dje, K. B., Diedhiou, A., Kouassi, K. L., Kamagate, B., Paturel, J.-E., Coulibaly, H. S. J.-P., Kouadio, C. A. K., Coulibaly, T. J. H., Konate, D., Didi, S. R., Dje, K. B., Diedhiou, A., Kouassi, K. L., Kamagate, B., Paturel, J.-E., Coulibaly, H. S. J.-P., Kouadio, C. A. K., & Coulibaly, T. J. H. (2023). Observed Changes in Rainfall and Characteristics of Extreme Events in Côte d'Ivoire (West Africa). *Hydrology 2023, Vol. 10*, *10*(5). https://doi.org/10.3390/HYDROLOGY10050104
Koubodana, na H., Tall, M., Amoussou, E., Mumtaz, M., Adounkpe, J., & Atchonouglo, K. (2019). *Trend Analysis of Hydroclimatic Historical Data and Future Scenarios of Climate Extreme Indices over Mono River Basin in West Africa*. https://doi.org/10.20944/preprints201906. 0267.v1
Lawin, A. E., Houngue̖, N. R., Biaou, C. A., Badou, D. F., Emmanuel, L. A., Hounguè, N. R., Biaou, C. A., & Badou, D. F. (2019). Statistical Analysis of Recent and Future Rainfall and Temperature Variability in the Mono River Watershed (Benin, Togo). *Climate 2019, Vol. 7*, *7*(1). https://doi.org/10.3390/CLI7010008
M'Po, Y. N., Lawin, E. A., Yao, B. K., Oyerinde, G. T., Attogouinon, A., & Afouda, A. A. (2017). Decreasing Past and Mid-Century Rainfall Indices over the Ouémé River Basin, Benin (West Africa). *Climate 2017, Vol. 5*, *5*(3), 74. https://doi.org/10.3390/cli5030074
Mahe, G., Lienou, G., Descroix, L., Bamba, F., Paturel, J. E., Laraque, A., Meddi, M., Habaieb, H., Adeaga, O., Dieulin, C., Chahnez Kotti, F., & Khomsi, K. (2013). The rivers of Africa: Witness of climate change and human impact on the environment. *Hydrological Processes*, *27*(15), 2105–2114. https://doi.org/10.1002/hyp.9813
Martinich, J., & Crimmins, A. (2019). Climate damages and adaptation potential across diverse sectors of the United States. *Nature Climate Change 2019 9:5*, *9*(5), 397–404. https://doi.org/10.1038/s41558-019-0444-6
Milinski, S., Maher, N., & Olonscheck, D. (2020). How large does a large ensemble need to be? *Earth System Dynamics*, *11*(4), 885–901. https://doi.org/10.5194/esd-11-885-2020
Ogbu, K. N., Hounguè, N. R., Gbode, I. E., & Tischbein, B. (2020). Performance evaluation of satellite-based rainfall products over Nigeria. *Climate*, *8*(10), 1–23. https://doi.org/10.3390/CLI8100103
Rholan, N., Delos, A., Almoradie, S., & Evers, M. (2022). *A Multi Criteria Decision Analysis Approach for Regional Climate Model Selection and Future Climate Assessment in the Mono River Basin, Benin and Togo*.
Sen, P. K. (1968). Estimates of the Regression Coefficient Based on Kendall's Tau. *Journal of the American Statistical Association*, *63*(324), 1379–1389. https://doi.org/10.1080/01621459.1968.10480934
Şen, Z. (2011). Innovative Trend Analysis Methodology. *Journal of Hydrologic Engineering*, *17*(9), 1042–1046. https://doi.org/10.1061/(asce)he.1943-5584.0000556
Şen, Z. (2015). Innovative trend significance test and applications. *Theoretical and Applied Climatology 2015 127:3*, *127*(3), 939–947. https://doi.org/10.1007/s00704-015-1681-x
Shuaifeng, S., & Xiaodong, Y. (2022). Projected changes and uncertainty in cold surges over northern China using the CMIP6 weighted multi-model ensemble. *Atmospheric Research*, *278*, 106334. https://doi.org/10.1016/j.atmosres.2022.106334
Sidibe, M., Dieppois, B., Eden, J., Mahé, G., Paturel, J. E., Amoussou, E., Anifowose, B., Van De Wiel, M., & Lawler, D. (2020). Near-term impacts of climate variability and change on hydrological systems in West and Central Africa. *Climate Dynamics 2020 54:3*, *54*(3), 2041–2070. https://doi.org/10.1007/s00382-019-05102-7
Sylla, M. B., Giorgi, F., Pal, J. S., Gibba, P., Kebe, I., & Nikiema, M. (2015). Projected Changes in the Annual Cycle of High-Intensity Precipitation Events Over West Africa for the Late Twenty-First Century. *Journal of Climate*, *28*(16), 6475–6488. https://doi.org/10.1175/JCLI-D-14-00854.1
Taye, M. T., Dyer, E., Charles, K. J., & Hirons, L. C. (2021). Potential predictability of the Ethiopian summer rains: Understanding local variations and their implications for water management decisions. *Science of The Total Environment*, *755*, 142604. https://doi.org/10.1016/J.SCITOTENV.2020.142604
Upadhyay, R. K., & Upadhyay, R. K. (2020). Markers for Global Climate Change and Its Impact on Social, Biological and Ecological Systems: A Review. *American Journal of Climate Change*, *9*, 159–203. https://doi.org/10.4236/ajcc.2020.93012
Wu, H., & Qian, H. (2017). Innovative trend analysis of annual and seasonal rainfall and extreme values in Shaanxi, China, since the 1950s. *International Journal of Climatology*, *37*(5), 2582-2592.

Zhang, X., Alexander, L., Hegerl, G. C., Jones, P., Tank, A. K., Peterson, T. C., Trewin, B., & Zwiers, F. W. (2011). Indices for monitoring changes in extremes based on daily temperature and precipitation data. *Wiley Interdisciplinary Reviews: Climate Change*, *2*(6), 851–870. https://doi.org/10.1002/WCC.147